JGR Space Physics

RESEARCH ARTICLE
10.1029/2025JA034763

Relationship Between Magnetosheath ULF Waves and Ground-Based Pc3-4 Waves: A Statistical Study

Terry Zixu Liu[1], Vassilis Angelopoulos[1], Seth Dorfman[2,3], Michael D. Hartinger[1,2], Savvas Raptis[4], Kun Zhang[1,5], and Siqi Zhao[6]

[1]Department of Earth, Planetary, and Space Sciences, University of California, Los Angeles, CA, USA, [2]Space Science Institute, Boulder, CO, USA, [3]Department of Physics and Astronomy, University of California, Los Angeles, CA, USA, [4]Applied Physics Laboratory, Johns Hopkins University, Laurel, MD, USA, [5]Department of Physical Sciences, Embry-Riddle Aeronautical University, Daytona Beach, FL, USA, [6]Institute of Physics and Astronomy, University of Potsdam, Potsdam, Germany

Abstract Foreshock ultralow frequency (ULF) waves are a major contributor to magnetospheric Pc3–4 waves (7–100 mHz), but their transmission through the magnetosheath is not well understood. Using 109 THEMIS traversals from the bow shock to the magnetopause, in conjunction with ground magnetometer (GMAG) measurements, we performed a statistical analysis of magnetosheath ULF waves and their relationship to ground-based Pc3–4 waves. Our findings reveal that in quasi-parallel regions, magnetic and dynamic pressure wave power are correlated with ground-based magnetic wave power at periods of ∼30s, with correlation coefficients reaching up to ∼0.7. The correlation depends on the THEMIS spacecraft's position in the magnetosheath as well as the magnetic local time and latitude of the ground stations. In contrast, in quasi-perpendicular regions, the correlation is weaker (up to ∼0.3) and increases with decreasing frequency. Additionally, in quasi-perpendicular regions, wave power increases from the bow shock to the magnetopause, consistent with local excitation, whereas waves in quasi-parallel regions are less compressive with power relatively stable, consistent with a foreshock origin. Our results suggest that foreshock-originated waves in quasi-parallel regions contribute more effectively to magnetospheric ULF waves than those in quasi-perpendicular regions, through both magnetic field and dynamic pressure oscillations, with a preferential propagation from the dawnside magnetosheath to both sides of the magnetosphere.

Plain Language Summary Ultralow-frequency (ULF) waves with periods of ∼30s are commonly observed in Earth's magnetosphere and are usually driven by foreshock ULF waves. However, how these waves travel through the magnetosheath and enter the magnetosphere is not fully understood. In this study, we investigate how magnetosheath ULF waves are related to magnetospheric ULF waves inferred from ground magnetometers. Using more than 100 spacecraft crossings of the magnetosheath, we show that waves originating from the foreshock are strongly linked to geomagnetic waves with periods of ∼30s. This connection is strongest when the spacecraft is close to the magnetopause and is more pronounced on the dawnside. In contrast, waves locally generated in the magnetosheath show only weak connections to ground observations. We also find that both magnetic field fluctuations and dynamic pressure variations in the magnetosheath contribute to driving geomagnetic waves. These results demonstrate that foreshock-induced waves can survive passage through the magnetosheath and efficiently drive magnetospheric ULF waves, while locally generated magnetosheath waves play a more limited role.

Key Points:

- Wave power in the quasi-parallel magnetosheath region correlates with ground-based wave power at ∼30s period with coefficients up to ∼0.7
- Correlation coefficients depend on spacecraft position in the magnetosheath and magnetic local time and latitude of ground stations
- Wave power in the quasi-perpendicular magnetosheath region weakly correlates with ground-based wave power with coefficients up to ∼0.3

Supporting Information:

Supporting Information may be found in the online version of this article.

Correspondence to:

T. Z. Liu,
terryliuzixu@ucla.edu

Citation:

Liu, T. Z., Angelopoulos, V., Dorfman, S., Hartinger, M. D., Raptis, S., Zhang, K., & Zhao, S. (2026). Relationship between magnetosheath ULF waves and ground-based Pc3-4 waves: A statistical study. *Journal of Geophysical Research: Space Physics*, *131*, e2025JA034763. https://doi.org/10.1029/2025JA034763

Received 10 OCT 2025
Accepted 18 FEB 2026

Author Contributions:

Conceptualization: Terry Zixu Liu
Data curation: Terry Zixu Liu
Formal analysis: Terry Zixu Liu
Funding acquisition: Terry Zixu Liu, Kun Zhang
Investigation: Terry Zixu Liu, Vassilis Angelopoulos, Seth Dorfman, Michael D. Hartinger, Savvas Raptis, Kun Zhang
Methodology: Terry Zixu Liu
Resources: Siqi Zhao
Supervision: Vassilis Angelopoulos
Validation: Terry Zixu Liu
Visualization: Terry Zixu Liu
Writing – original draft: Terry Zixu Liu
Writing – review & editing: Terry Zixu Liu, Vassilis Angelopoulos, Seth Dorfman, Michael D. Hartinger, Savvas Raptis, Siqi Zhao

1. Introduction

Magnetospheric ultralow frequency (ULF) waves play a crucial role in coupling energy across the magnetosphere and ionosphere (see review by Takahashi et al., 2006), making it essential to understand their generation mechanisms. Magnetospheric Pc3-4 waves (7–100 mHz) are widely believed to originate from wave transmission from the ion foreshock, as they preferentially occur at low interplanetary magnetic field (IMF) cone angles (e.g., Greenstadt & Olson, 1976; Russell et al., 1983; Takahashi et al., 1984). When the IMF is quasi-parallel to the bow shock normal (i.e., angle between them $\theta_{Bn} < 45°$), some solar wind ions are reflected (e.g., Sonnerup, 1969) and some magnetosheath ions can leak out (e.g., Edmiston et al., 1982; Liu et al., 2024), forming the ion foreshock (see review by Eastwood et al., 2005; Burgess et al., 2012). These reflected ions can interact with incoming solar wind ions to excite ULF waves, including the commonly observed "30s waves" (see

review by Wilson, 2016). Foreshock ULF waves are then convected by the supersonic solar wind, modulate the bow shock's compression ratio, and generate waves in the magnetosheath propagating toward the magnetopause (Turc et al., 2023), ultimately generating Pc3-4 waves in the magnetosphere. This connection between foreshock ULF waves and Pc3-4 waves has been confirmed through case studies using conjunction observations (e.g., Clausen et al., 2009; Engebretson et al., 1987; Takahashi et al., 2021).

A recent statistical study by Liu et al. (2025) demonstrates that foreshock wave power and magnetospheric wave power, inferred from ground magnetometers (GMAG), follow a power-law relationship, with peak correlation coefficients exceeding 0.5 at periods of ∼30s. Their results indicate that foreshock ULF waves are more likely to be transmitted from the local bow shock than from the subsolar point. Their study also suggests transmission across a broad range of magnetic local time (MLT). In contrast, correlation coefficients between solar wind and ground-based ULF wave power increase only up to ∼0.3 as frequency decreases within the Pc3–4 bands, consistent with the solar wind being a typical driver of the lower frequency, Pc5 wave band (∼1–7 mHz; e.g., Eriksson et al., 2006; Stephenson & Walker, 2002).

However, how foreshock-induced waves are transmitted across the magnetosheath is not well understood. Recent observations by Zou et al. (2025) showed stronger fluctuations in the subsolar magnetosheath under more radial IMF, confirming the contribution of foreshock-originated waves to the magnetosheath waves downstream of quasi-parallel bow shocks, which are expected to drive magnetospheric Pc3-4 waves. Additionally, downstream of quasi-perpendicular bow shocks, the temperature anisotropy in the magnetosheath can also locally excite Alfvén and mirror mode waves (e.g., Lacombe & Belmont, 1995; Omidi et al., 1994). It is unknown whether such locally generated magnetosheath waves contribute to magnetospheric ULF waves. If they do contribute, their relative contribution compared to external foreshock waves is also unknown. To investigate these questions, we conducted a statistical study using data from the Time History of Events and Macroscale Interactions during Substorms (THEMIS, Angelopoulos, 2008) spacecraft, across the magnetosheath from the bow shock to the magnetopause, in conjunction with GMAG measurements. Section 2 describes the database and methodology, Section 3 presents the results, and Sections 4 and 5 provide the discussion and conclusions.

2. Data and Methods

We utilize data from the TH-A spacecraft with an apogee of ∼13 R_E to observe the dayside magnetosheath during the period 2016–2020. Magnetic field and plasma measurements were obtained from a fluxgate magnetometer (FGM; Auster et al., 2008) and an electrostatic analyzer (ESA; McFadden et al., 2008). To determine the spacecraft position relative to the bow shock and magnetopause, we manually identified 109 magnetosheath time intervals during which TH-A crossed both the bow shock and the magnetopause in fast survey mode (with FGM resolution of 0.0625 s and ESA resolution of 2.74 s). These observations are mainly between ∼10 and ∼14hr MLT (see Figure 1f). The event list can be found in the Supporting Information S1. Figure 1 shows an example of a magnetosheath time interval, with bow shock and magnetopause crossings marked by vertical dotted lines.

To determine the relative spacecraft position within the magnetosheath, we calculate the normalized distance $d = (r_{bs} - r_{sc})/(r_{bs} - r_{mp})$, where r_{sc}, r_{bs}, and r_{mp} represent the radial positions of TH-A at a given time, during the bow shock crossing, and during the magnetopause crossing, respectively (e.g., Figure 1d). This coordinate has its 0 at the bow shock and increases to a value of 1 at the magnetopause. This method is generally more accurate than using empirical bow shock and magnetopause models (e.g., Figure 1e). In some cases, bow shock and magnetopause oscillations cause multiple crossings. To avoid including time intervals in the solar wind (characterized by low field strength, low density, and high flow speed) or magnetosphere (characterized by strong northward B_z, very low density, and low flow speed), we use the last crossing into and the first crossing out of the magnetosheath (though this approach slightly underestimates the magnetosheath thickness). Although this method has defects and uncertainties, it is sufficient in this study to distinguish magnetosheath regions close to the bow shock and close to the magnetopause, rendering potentially large uncertainties innocuous.

Within the magnetosheath, we apply a 5-min sliding window with a 2.5 min step size to calculate the power spectra of the magnetic field and plasma parameters, using a frequency bin size of 0.01 Hz. For each time window, we use GMAG stations across different magnetic latitudes (MLAT) and within ±6 h MLT relative to TH-A, to remotely infer magnetospheric ULF wave power. We utilize THEMIS (UCLA) GMAG data (Russell et al., 2009) as well as other GMAG networks (e.g., CARISMA and USGS). Because 1s resolution is required for GMAG

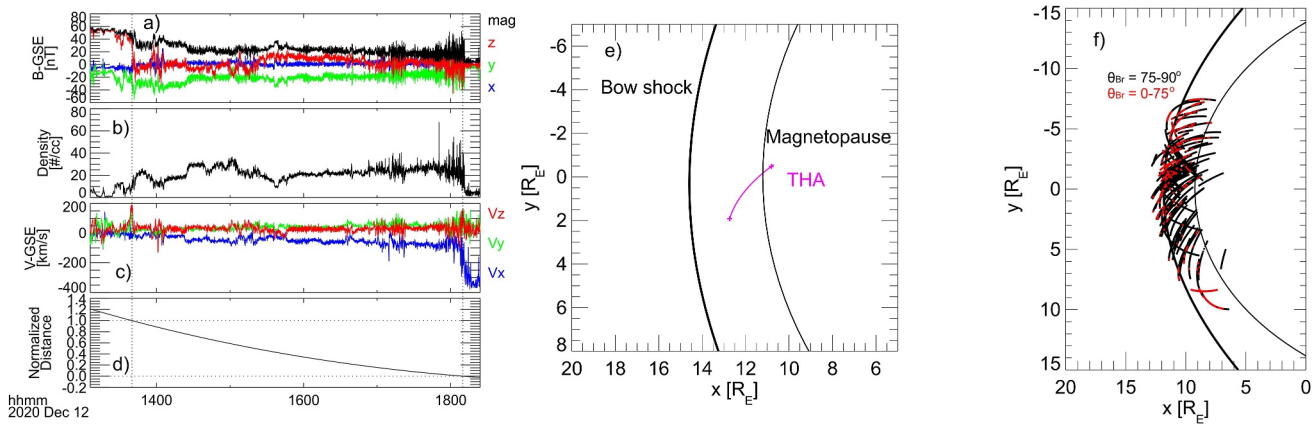

Figure 1. TH-A observation example of a magnetosheath time interval: (a) magnetic field in GSE, (b) ion density, (c) ion bulk velocity, and (d) normalized distance relative to the bow shock and magnetopause (from 0 to 1), defined in the text. Vertical dotted lines indicate the magnetopause and bow shock. Panel (e) demonstrates the orbit of TH-A during the magnetosheath traversing, relative to the model bow shock (Merka et al., 2005) and model magnetopause (Shue et al., 1998) in the equatorial plane, using solar wind parameters measured by TH-B at the lunar orbit. Crosses indicate the observed locations of bow shock and magnetopause crossings, which deviate from the models. Although TH-A is off the equator by ~2 R_E, it is insufficient to explain this large discrepancy. Panel (f) shows the spacecraft trajectory of all the events. Red indicates time intervals for θ_{Br} = 0–75°. Note that the trajectory at X ~ 6–9 R_E and Y ~ 6–10 R_E without clear bow shock crossing is due to the overlapping of three different events.

measurements, available GMAG stations are primarily located in North America (see spatial distribution in Figure S1 of Supporting Information S1). We thus focus on an MLAT range of 40–70°. Due to the limited station coverage, not all magnetosheath intervals have corresponding GMAG measurements (e.g., only about half when we restrict MLT separation between TH-A and GMAG stations to ±2 h). We then compare magnetosheath and ground-based wave power at each time window and calculate Spearman correlation coefficients at each frequency (which assesses the monotonic relationships). We mainly compare total wave power, though results for compressional components in the magnetosheath and individual components on the ground (north–south, east–west, and vertical components) are also examined. We consider correlation coefficients of 0.6–0.8 as strong, 0.4–0.6 as moderate, 0.2–0.4 as weak, and 0–0.2 as no correlation.

It is important to distinguish between magnetosheath regions downstream of quasi-parallel and quasi-perpendicular bow shocks in order to highlight foreshock-induced waves. Karlsson et al. (2021) provided a comprehensive classification method of these regions, based on suprathermal ion intensity and magnetic field fluctuations. However, we do not use this method because the magnetic field fluctuations we analyze should be independent of the classification method. Instead, we use the angle θ_{Br} between the 5-min averaged magnetic field in the magnetosheath and the radial direction as a proxy for θ_{Bn} in the magnetosheath.

According to the Rankine-Hugoniot relations, for a high-Mach number shock with an upstream θ_{Bn} of 45°, the downstream θ_{Bn} is ~75°. (For a quick estimate: the normal component of magnetic field remains constant across the shock, while the tangential component increases by a factor of slightly less than 4, changing θ_{Bn} from $\tan^{-1}1 = 45°$ to slightly less than $\tan^{-1}4 = 76°$). Thus, θ_{Br} = 0–75° (75–90°) roughly corresponds to regions downstream of quasi-parallel (quasi-perpendicular) bow shocks. Because magnetic field lines tend to drape azimuthally, θ_{Br} deeper in the magnetosheath likely overestimates θ_{Bn} just downstream of the shock. In our events, θ_{Br} = 0–75° regions occur more frequently on the dawnside (as suggested by Figure 1f), and their sampling rate decreases from 9 to 14hr MLT (Figure S2 in Supporting Information S1), consistent with the ion foreshock's dawnside preference under the IMF's Parker spiral geometry. In the next section, we examine how different θ_{Br} ranges affect the results.

3. Results

3.1. Correlation Between TH-A and GMAG Measurements

We first compare the total magnetic wave power at 0.037 Hz (~30s wave period) in the magnetosheath with that from GMAG stations. Each magnetosheath wave power calculation can correspond to multiple ground-based wave power observations, measured at GMAG stations located at different MLATs and MLTs, resulting in

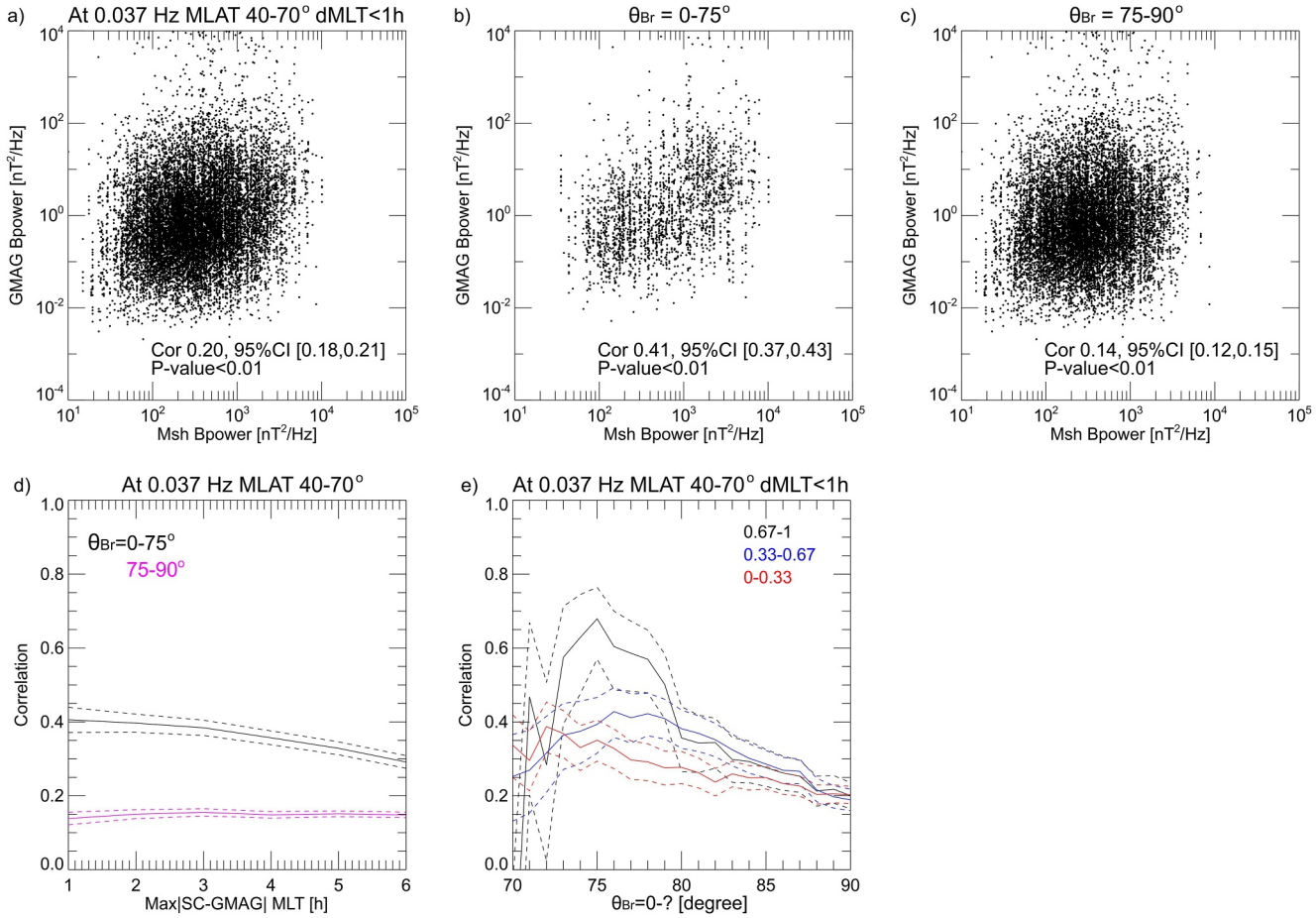

Figure 2. Magnetic wave power measured by TH-A in the magnetosheath versus magnetic wave power measured by GMAG stations with MLAT of 40–70° and MLT separations from TH-A within ±1 h, at 0.037 Hz. Panels (a) are all events, and panels (b, c) are events separated by θ_{Br} = 0–75° and 75–90°, respectively. Spearman correlation coefficient, 95% confidence interval, and P-value are labeled in each panel. Panel (d) shows Spearman correlation coefficients as a function of MLT separations between TH-A and GMAG stations for θ_{Br} = 0–75° (black) and 75–90° (magenta). Panel (e) shows Spearman correlation coefficients as a function of θ_{Br} range from 0° to different values, at three normalized distances from the bow shock to the magnetopause, indicated by red (0–0.33), blue (0.33–0.67), and black (0.67–1). Dashed lines indicate 95% confidence intervals.

the appearance of vertical stripe features in Figure 2. A detailed examination of the dependence on MLAT and MLT is presented later.

In Figure 2a, the correlation between magnetosheath wave power and ground-based wave power is rather weak, with a correlation coefficient of 0.20. However, when we categorize magnetosheath regions based on θ_{Br}, the correlation coefficient improves to 0.41 for θ_{Br} = 0–75° (Figure 2b). For θ_{Br} = 75–90°, on the other hand, the correlation coefficient decreases to 0.14 (Figure 2c). In Figures 2a–2c, we limited the MLT separations between TH-A and GMAG stations to be within ±1 h, because Figure 2d shows that for θ_{Br} = 0–75°, the correlation coefficient increases with decreasing MLT separations, consistent with that for foreshock ULF waves (Liu et al., 2025). For θ_{Br} = 75–90°, there is no clear dependence on MLT separations, consistent with that for solar wind ULF waves.

We further assess how variations in the θ_{Br} range affect correlation at three normalized distances from the bow shock to the magnetopause. Figure 2e shows that narrowing the range from (0°, 90°) to around (0°, 75°) improves the correlation. Further narrowing the range reduces the correlation and increases uncertainty due to fewer events. Especially near the magnetopause (black), the correlation rises sharply at (0°, 80°), likely reflecting the magnetosheath counterpart of foreshock boundaries (typically beyond θ_{Bn} = 45°; e.g., Karlsson et al., 2021). Around (0°, 75°), the correlation increases markedly from the bow shock (<0.4) to the magnetopause (~0.7). This improved correlation occurs likely because the wave power measured closer to the magnetopause better

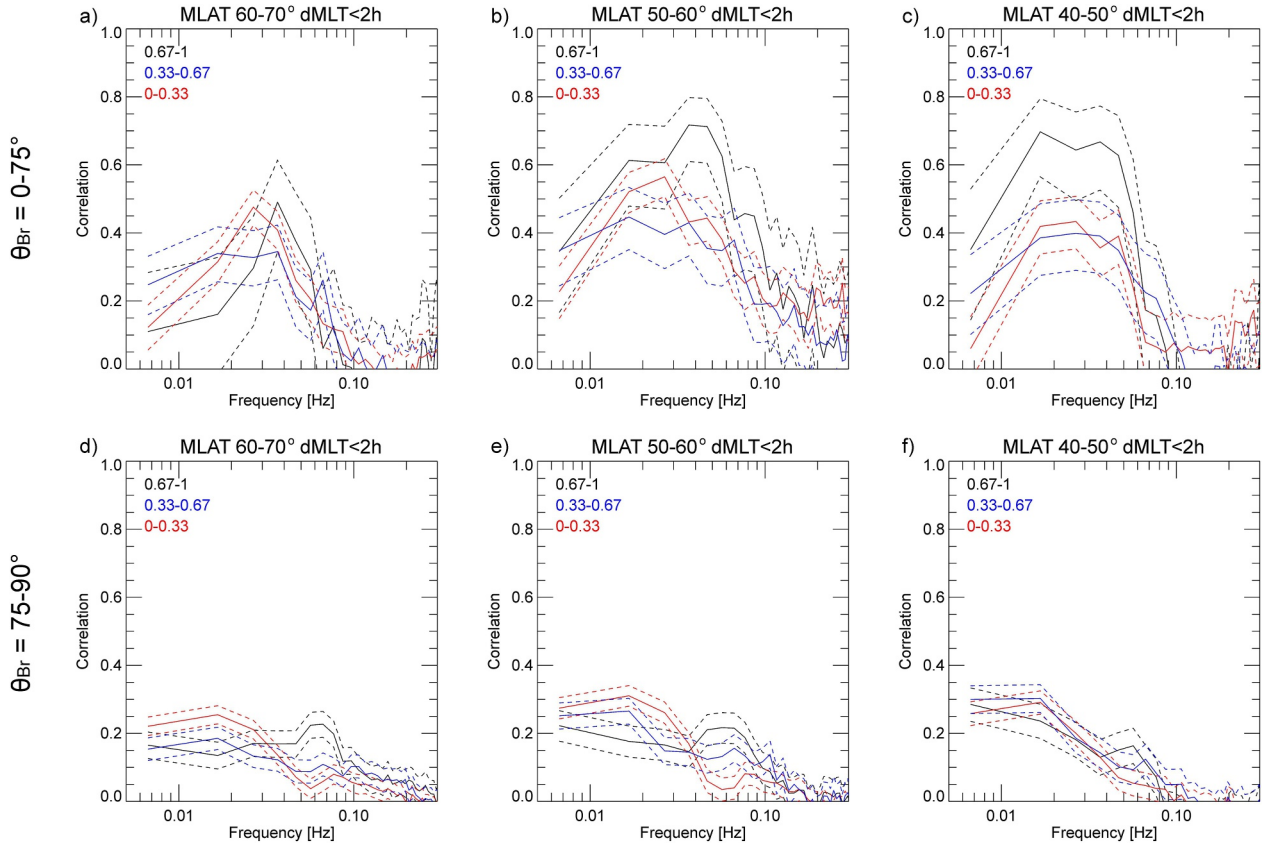

Figure 3. Spearman correlation coefficients versus frequency at three normalized distances from the bow shock to the magnetopause, indicated by red (0–0.33), blue (0.33–0.67), and black (0.67–1). Dashed lines indicate 95% confidence intervals. Panels (a) to (c) are for θ_{Br} = 0–75° with GMAG stations at 60–70°, 50–60°, and 40–50° MLAT, respectively. Panels (d, f) are for θ_{Br} = 75–90° with GMAG stations at 60–70°, 50–60°, and 40–50° MLAT, respectively. The MLT separation between the TH-A and GMAG stations is within ±2 h. For θ_{Br} = 0–75°, the correlation does not increase monotonically from the bow shock to the magnetopause, partly because how θ_{Br} ranges (Figure 2e) and MLT separations (Figure S5 in Supporting Information S1) affect correlation depends on the radial distance.

represents the true wave signal entering the magnetosphere. Before reaching the magnetopause, the waves may undergo modifications due to factors such as wave evolution and Doppler shift. In addition, measurements taken farther from the magnetopause can introduce larger timing and MLT uncertainties relative to the actual wave input. From (0°, 80°) to (0°, 90°), on the other hand, the correlation shows little dependence on normalized distance. As (0°, 75°) yields the strongest correlation, we adopt it to categorize magnetosheath regions for both scientific and practical purposes (although near the magnetopause, it may not correspond exactly to upstream θ_{Bn} = 45° due to field line draping).

Therefore, it is very likely that θ_{Br} = 0–75° regions are dominated by waves from the ion foreshock, whereas θ_{Br} = 75–90° regions are more dominated by waves from the solar wind and local excitation in the magnetosheath. Figure 2 thus suggests that foreshock-originated waves could contribute more effectively to magnetospheric ULF waves (inferred from GMAG measurements) at periods of ∼30s than solar wind-originated waves and magnetosheath-generated waves.

Next, we examine how wave frequency affects the magnetosheath-to-ground correlation. We use MLT separations within ±2 hr to ensure a sufficient sample size. Figure 3 shows the correlation coefficient as a function of frequency for GMAG stations located at various MLATs. In the θ_{Br} = 0–75° region (Figures 3a–3c), the correlation peaks around the 30s wave period, similar to the foreshock-to-ground relationship (Liu et al., 2025). This frequency dependence further confirms that wave power in this region is dominated by foreshock-induced waves. Additionally, the strongest correlation occurs when TH-A is near the magnetopause (black), consistent with Figure 2e. Near the magnetopause, the peak correlation is stronger for GMAG stations at MLAT of 40–50° and 50–60° (∼0.7) than for those at 60–70° (∼0.5). Near the bow shock (red), the peak correlation can reach ∼0.5,

comparable to the foreshock-to-ground correlation (Liu et al., 2025), suggesting that crossing the bow shock may not significantly affect the correlation.

In contrast, the correlation for θ_{Br} = 75–90° is weak (up to ∼0.3) and shows no clear dependence on radial position (Figures 3d–3f). There is a trend of increasing correlation with decreasing frequency (minimum frequency 6.67 mHz), similar to the solar wind-to-ground relationship (Liu et al., 2025). This trend is likely because transmitted solar wind disturbances become more influential at lower frequencies, as a typical driver of Pc5 waves (e.g., Sibeck et al., 1989). There is likely a secondary peak at ∼0.06 Hz with increasing correlation from the bow shock (red) to the magnetopause (black) across all three MLAT ranges, different from the solar wind-to-ground relationship. This secondary peak possibly implies contributions from a wave population locally generated in the magnetosheath. One candidate is magnetic mirror modes (e.g., Omidi et al., 1994), which occur and grow preferentially in the quasi-perpendicular magnetosheath (Soucek et al., 2015) with a mean period of ∼12s (Soucek et al., 2008).

In Figure 2b, the relationship between magnetosheath wave power P_M and ground-based wave power P_G for θ_{Br} = 0–75° can be fitted with a power law, $P_G = b \cdot P_M^a$, where factors a and b are obtained through linear regression on log-log scales. Figure S3 in Supporting Information S1 shows factors a and b as functions of frequency. Overall, a and b are larger than those between upstream and ground-based wave power, while exhibiting a similar frequency dependence (Liu et al., 2025; see examples of linear regression in Figure S4 of Supporting Information S1). The larger fitted factors suggest that transmission of waves from the magnetosheath into the magnetosphere is more efficient than from the foreshock or solar wind, which is reasonable.

Next, we examine how the correlation at 0.037 Hz depends on the MLT of TH-A and ground stations. Although Figure 2d shows that smaller MLT separations generally favor stronger correlation for θ_{Br} = 0–75°, this dependence becomes more complicated close to the magnetopause (normalized distance 0.5–1; see Figure S5 in Supporting Information S1). To further illustrate the MLT dependence, Figure 4 shows the correlation as a function of the MLT of both TH-A and ground stations. For θ_{Br} = 0–75°, near the bow shock (normalized distance 0–0.5), the correlation is stronger near the center without a clear pattern (Figures 4a–4c). This may be because, immediately after foreshock ULF waves enter the magnetosheath, they can propagate in various directions, leading to a weak MLT dependence.

Close to the magnetopause (normalized distance 0.5–1), the MLT dependence becomes clearer (Figures 4d–4f), likely because the wave propagation pattern to the ground becomes more certain. First, there is a clear dawn-dusk asymmetry associated with the MLT of TH-A (Figures 4d–4f). This asymmetry may be caused by the higher occurrence of quasi-parallel regions on the dawnside due to Parker spiral geometry (Figure S2 in Supporting Information S1). Second, when GMAG stations are located at 60–70° MLAT, the dependence on their MLT is not very clear (Figure 4d). At lower MLAT, however, stronger correlation occurs when GMAG stations are located on the duskside (Figure 4e) or on both the dawnside and duskside (Figure 4f). As TH-A moves from the dawnside toward noon, this MLT preference progressively shifts away from noon, increasing at both dusk and dawn. This pattern may result from the azimuthal propagation of ULF waves toward both the duskside and dawnside, as they reach deeper in the magnetosphere. Additionally, when the local standing Alfvén wave frequency at the GMAG MLT and MLAT matches the magnetosheath wave frequency (e.g., Singer et al., 1981), a higher correlation occurs, which may also contribute to the MLT-MLAT dependence.

For θ_{Br} = 75–90° in Figures 4g–4i and 4k, the MLT dependence resembles that in Figure 4e. There is a stronger correlation when TH-A is on the dawnside, even though the sampling rate of the θ_{Br} = 75–90° region is higher on the duskside. A possible explanation for this dawnside preference is that field-line draping along the magnetopause may cause the θ_{Br} = 75–90° region to include some foreshock-originated waves (e.g., Figure 2e). However, even when the θ_{Br} range is narrowed to 85–90°, a similar MLT dependence remained. Alternatively, this dependence may reflect general patterns of ULF wave propagation to the ground, and there could be an interplay between the wave source location and the properties of the magnetosphere-ionosphere system (e.g., global wave speeds that depend in part on variable plasma mass densities) that affects the wave propagation. e.g., previous studies examining diurnal trends in ground-based Pc3–4 wave power, regardless of the source mechanism, found that trends can vary depending on MLAT, frequency, season, and other factors (e.g., Bloom & Singer, 1995).

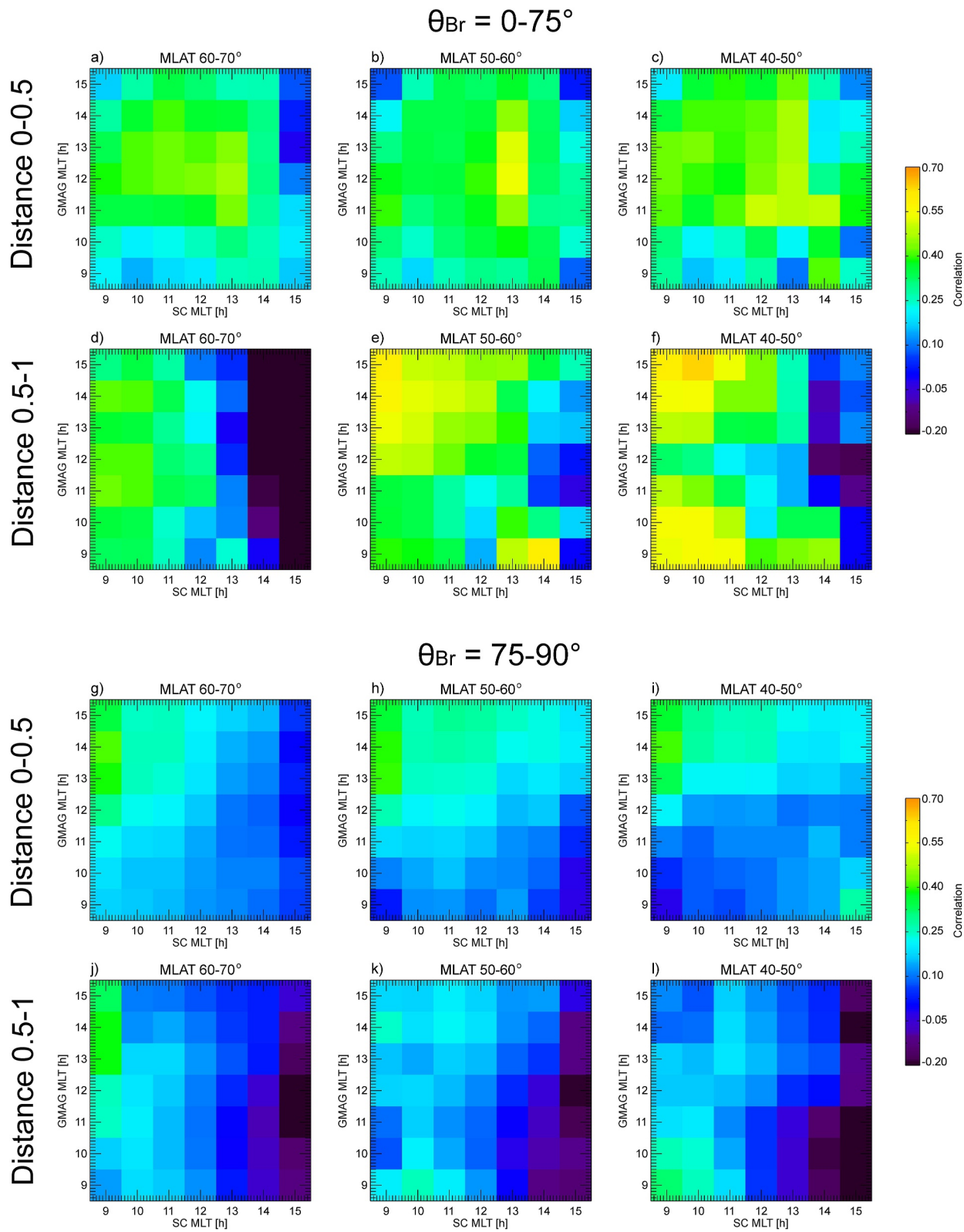

Figure 4. Correlation coefficients as a function of MLT between wave power from TH-A and from GMAG stations for $\theta_{Br} = 0–75°$ (top) and $\theta_{Br} = 75–90°$ (bottom). The three columns correspond to different MLAT ranges of GMAG stations. Panels (a–c) and (g–i) are for normalized distance from 0 to 0.5, and panels (d–f) and (j–l) are for normalized distance from 0.5 to 1. The bin size is 4 h MLT × 4 h MLT to ensure a sufficient sample size (more than tens of data points), with a shift of 1 h MLT.

3.2. Role of Dynamic Pressure Perturbation

How foreshock-induced waves cross the magnetopause remains an open question. One possible mechanism is the direct transmission of compressional waves. However, when we use only the compressional component of magnetosheath wave power (i.e., along the time-averaged field direction), the correlation coefficient with GMAG wave power decreases by ∼0.1 compared to using total wave power. This suggests that alternative mechanisms are likely involved in the magnetopause crossing. Another possible mechanism is dynamic pressure perturbations that locally perturb the magnetopause, thereby exciting ULF waves in the magnetosphere, ionosphere, and on the ground (e.g., Engebretson et al., 1991). To test this hypothesis, we correlate dynamic pressure wave power with ground-based magnetic wave power. Among the total dynamic pressure and its GSE-X component, the radial component shows the strongest correlation with ground-based wave power, especially near the magnetopause, possibly because the radial direction roughly aligns with the local magnetopause normal. Therefore, we focus on the radial component of dynamic pressure in the following analysis.

We first examine the correlation between plasma wave power and magnetic wave power in the magnetosheath at 0.037 Hz (same as Figure 2). In Figures 5a and 5b, radial dynamic pressure wave power shows a strong correlation with magnetosheath magnetic wave power in the $\theta_{Br} = 0–75°$ region but no correlation in the $\theta_{Br} = 75–90°$ region. When correlating density or radial velocity wave power with magnetosheath magnetic wave power, the correlation coefficients were 0.56 or 0.63 in the $\theta_{Br} = 0–75°$ region and 0.41 or 0.34 in the $\theta_{Br} = 75–90°$ region. The correlation coefficient between density and radial velocity wave power is ∼0.4 in the $\theta_{Br} = 0–75°$ region and ∼0 in the $\theta_{Br} = 75–90°$ region. The weaker correlation in the $\theta_{Br} = 75–90°$ region is likely due to the coexistence of multiple wave modes, including locally generated mirror and Alfvén modes (e.g., Lacombe & Belmont, 1995; Omidi et al., 1994) as well as solar wind-originated waves, each following different plasma–field relationships. In the $\theta_{Br} = 0–75°$ region, on the other hand, although foreshock ULF waves can generate magnetosheath waves through three mechanisms, shock reformation (e.g., Liu et al., 2021), mode conversion (e.g., Krauss-Varban, 1995), and modulation of shock's compression ratio, only the fast mode waves produced by the last mechanism can propagate deep into the magnetosheath and reach the magnetopause (Turc et al., 2023), leading to more coherent coupling between magnetic, density, and velocity perturbations.

Figures 5c and 5d compare radial dynamic pressure wave power with ground-based magnetic wave power in the same format as Figures 2b and 2c. The correlation coefficients are comparable to those in Figure 2 (using total dynamic pressure or x component decreases correlation by ∼0.04). Figures 6a–6c show that the correlation near the magnetopause for $\theta_{Br} = 0–75°$ is moderate or strong (0.5–0.7) over a broad frequency range below 0.1 Hz. Away from the magnetopause, correlation coefficients decrease. For $\theta_{Br} = 75–90°$, correlation coefficients increase up to ∼0.3 with decreasing frequency, with a secondary peak at ∼0.06 Hz near the magnetopause (Figures 6d–6f). As the correlation in Figure 6 is comparable to that in Figure 3, we conclude that both magnetic wave power and dynamic pressure wave power are likely important for driving magnetospheric ULF waves.

One might expect that the wave power of total pressure (including thermal, magnetic, and radial dynamic pressure) would exhibit a stronger correlation. However, there is no clear improvement compared to dynamic pressure alone. Additionally, the magnetic pressure wave power in the same data set as in Figure 2b yields a lower correlation coefficient (∼0.29). Therefore, the contribution of the wave field is likely not through its magnetic pressure. More comprehensive studies, including hybrid simulations, are needed to examine the interplay between magnetic and dynamic pressure perturbations in wave transmission across the magnetopause.

3.3. Wave Evolution in the Two Regions

Next, we examine how wave spectra evolve from the bow shock to the magnetopause by dividing the normalized distance into five bins. For each bin, we calculate the median as well as the 25th and 75th percentiles of wave power at each frequency to construct superposed spectra. Figure 7a shows that in the $\theta_{Br} = 0–75°$ region, the median spectra below 0.1 Hz exhibit little evolution with distance. In contrast, in the $\theta_{Br} = 75–90°$ region (Figure 7b), wave power below 0.1 Hz increases monotonically from the bow shock to the magnetopause. This difference is consistent with previous studies suggesting that magnetosheath-generated waves originate in source regions embedded in the magnetosheath and grow over time (e.g., Lacombe & Belmont, 1995; Omidi et al., 1994), whereas foreshock-originated waves transmitted through the bow shock likely cease growing and could be attenuated as they propagate further within the magnetosheath. Additionally, the wave power in the $\theta_{Br} = 0–75°$ region is stronger than that in the $\theta_{Br} = 75–90°$ region. This is consistent with the wave power

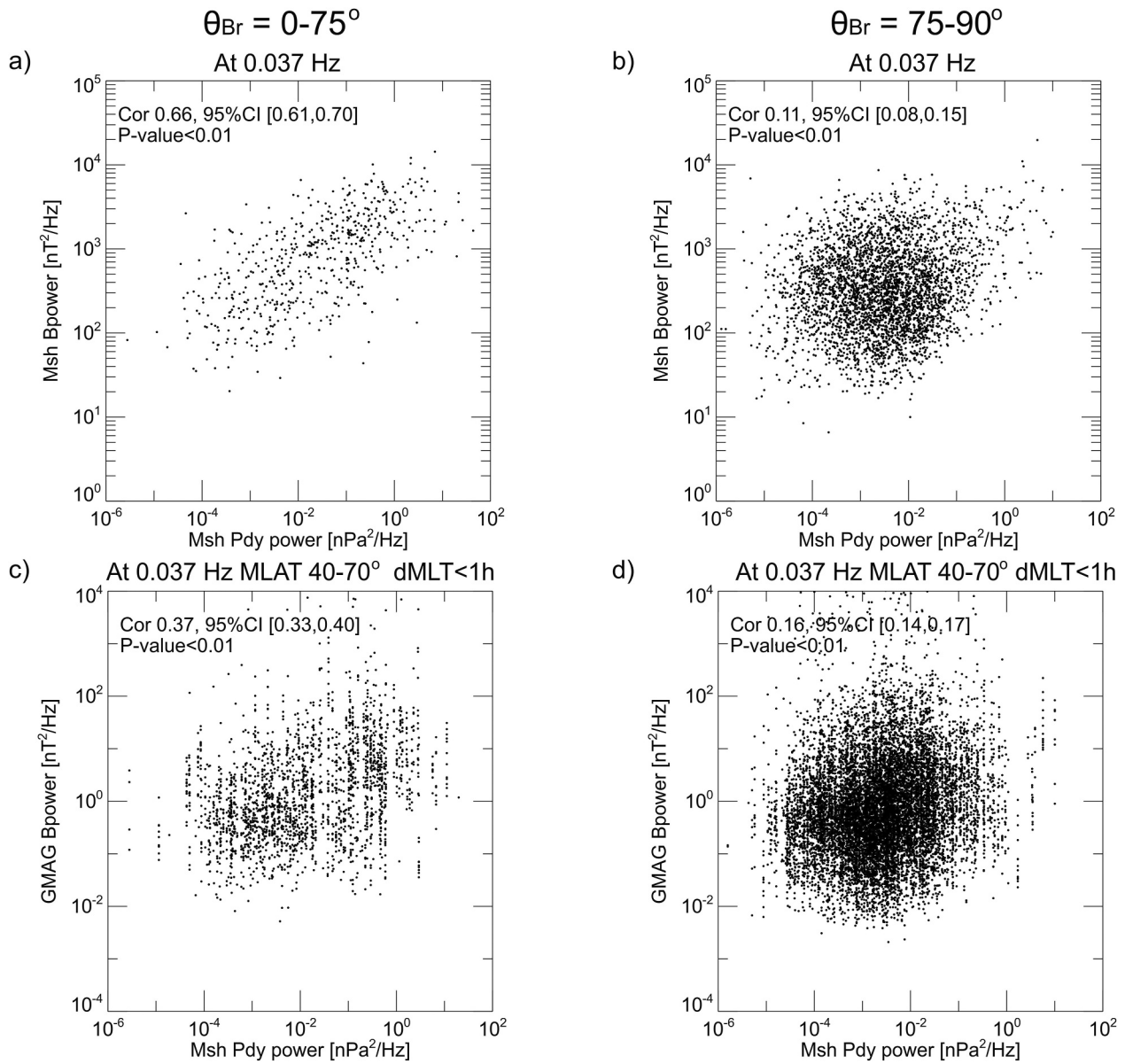

Figure 5. Dynamic pressure wave power at 0.037 Hz versus magnetic wave power in the magnetosheath (top panels) and measured by GMAG stations with MLAT of 40–70° and MLT separation from TH-A within ±1 h (bottom panels). The left and right panels are for θ_{Br} = 0–75°, and θ_{Br} = 75–90°, respectively. Spearman correlation coefficient, 95% confidence interval, and P-value are labeled in each panel.

differences between quasi-parallel and quasi-perpendicular regions, which have been used for classification (e.g., Karlsson et al., 2021; Koller et al., 2025; Raptis et al., 2020; Svenningsson et al., 2025). It is also notable that the wave power above 0.1 Hz shows different behaviors, but this is beyond the scope of this study. Superposed spectra corresponding to the upper and lower quartiles (Figure S6 in Supporting Information S1) support the same conclusions. Additionally, although wave power below 0.1 Hz in the θ_{Br} = 75–90° region increases toward the magnetopause, the correlation improves only near ∼0.06 Hz (Figures 3d–3f). Further investigation of the wave properties at 0.06 Hz is needed in the future.

Figure 8 compares the ratio of compressional wave power to total wave power using the same format as Figure 7. Below 0.1 Hz, waves in the θ_{Br} = 0–75° region are less compressive than those in the θ_{Br} = 75–90° region, consistent with previous results that foreshock 30s waves typically have large transverse components (see review by Wilson, 2016). In both regions, waves below 0.1 Hz are overall more compressive deeper in the magnetosheath

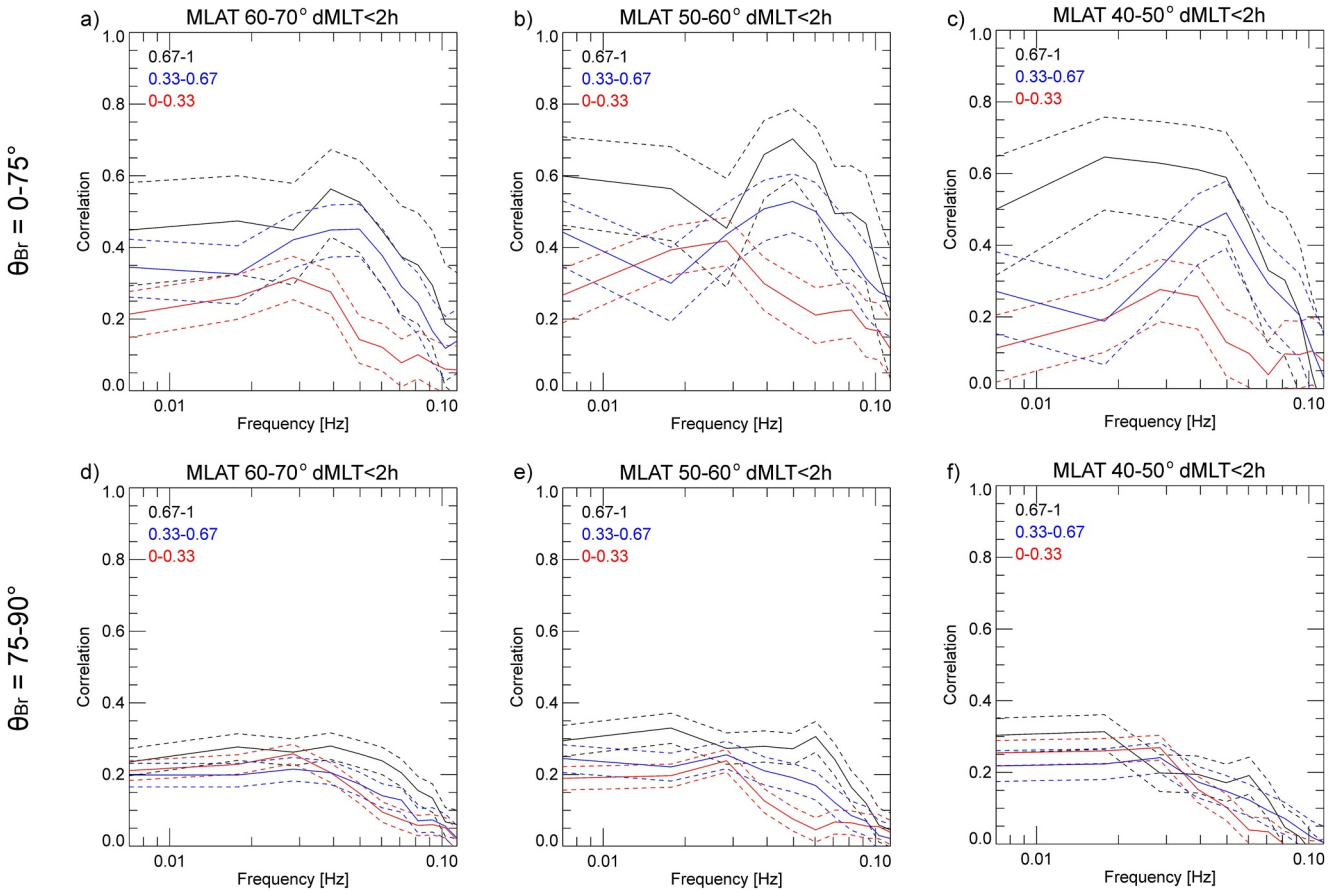

Figure 6. Spearman correlation coefficients between dynamic pressure wave power and GMAG-measured magnetic wave power, in the same format as Figure 3 except for a shorter frequency range due to lower time resolution.

(Above 0.1 Hz, waves become less compressive deeper in the magnetosheath in the θ_{Br} = 75–90° region). Figures 7 and 8 confirm that the θ_{Br} = 0–75° region is dominated by foreshock-induced waves, in contrast to the θ_{Br} = 75–90° region.

4. Discussion

Here, we summarize the comparison between magnetosheath-to-ground wave power relationships and upstream-to-ground wave power relationships (Liu et al., 2025). For θ_{Br} = 0–75°, both magnetosheath waves and foreshock ULF waves show peak correlation with ground waves at periods of ∼30s. Near the bow shock, magnetosheath-to-ground correlation is comparable to foreshock-to-ground correlation (∼0.5), and both are stronger at smaller MLT separations. Near the magnetopause, magnetosheath waves exhibit an even stronger correlation with ground waves (∼0.7, except for MLAT of 60–70°). Both magnetosheath waves near the magnetopause and foreshock ULF waves show stronger correlation when the spacecraft is on the dawnside for MLAT of 60–70° and GMAG stations are on either the duskside for MLAT of 50–60° or on both sides for MLAT of 40–50°. For θ_{Br} = 75–90°, both magnetosheath waves and solar wind ULF waves show stronger correlation with ground waves at lower frequencies (except at 0.06 Hz), without dependence on their MLT separation from the ground stations. This correlation is stronger when the GMAG stations are on the duskside and the spacecraft is on the dawnside for MLAT of 50–60° and 60–70°.

Based on these findings, we suggest that foreshock-originated waves with periods around 30s effectively contribute to magnetospheric ULF waves (inferred from GMAG measurements). This contribution may involve both magnetic field and dynamic pressure oscillations. The weak correlation in the θ_{Br} = 75–90° region does not necessarily indicate an absence of contribution. e.g., multiple wave populations may coexist in this region, each

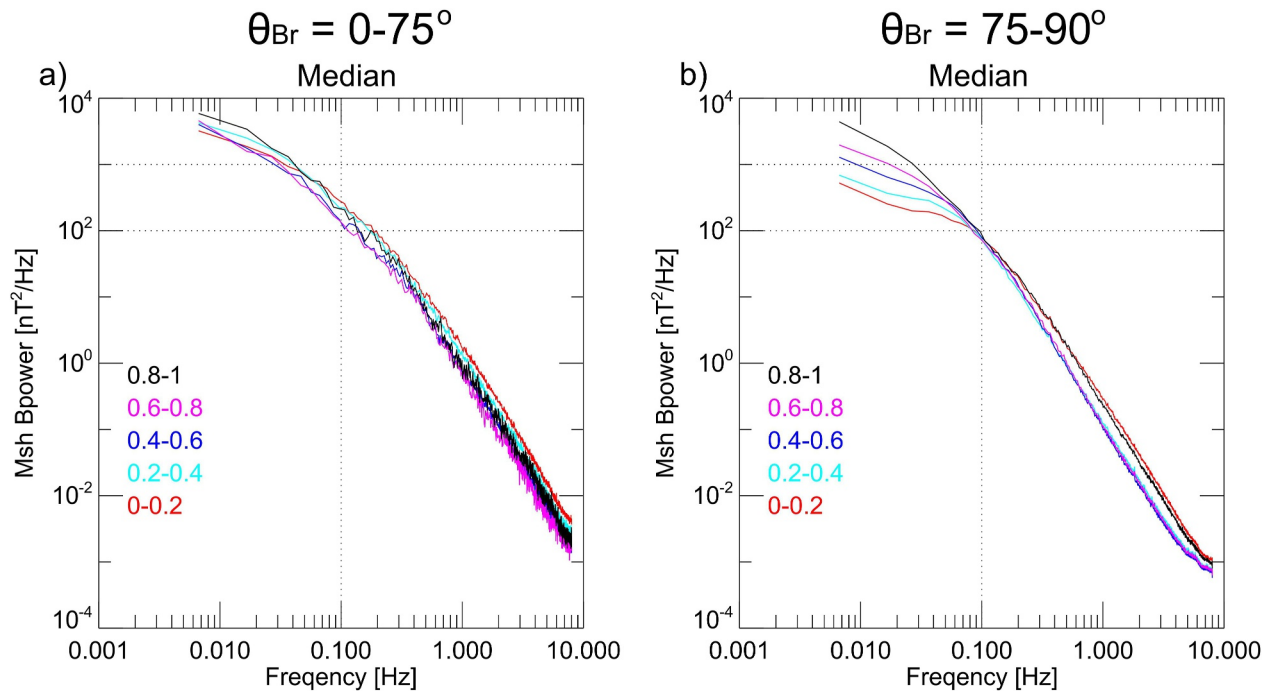

Figure 7. Superposed magnetic wave power spectra in the magnetosheath (median) versus frequency at five bins of normalized distance from the bow shock (0) to the magnetopause (1), for θ_{Br} = 0–75° (a) θ_{Br} = 75–90° (b). Vertical dotted lines indicate 0.1 Hz, and horizontal dotted lines are for comparison between panel (a) and panel (b).

correlating with GMAG measurements differently. When mixed, these modes may reduce the overall correlation. A more refined separation (e.g., isolating a potential wave population around 0.06 Hz) may reveal a better correlation.

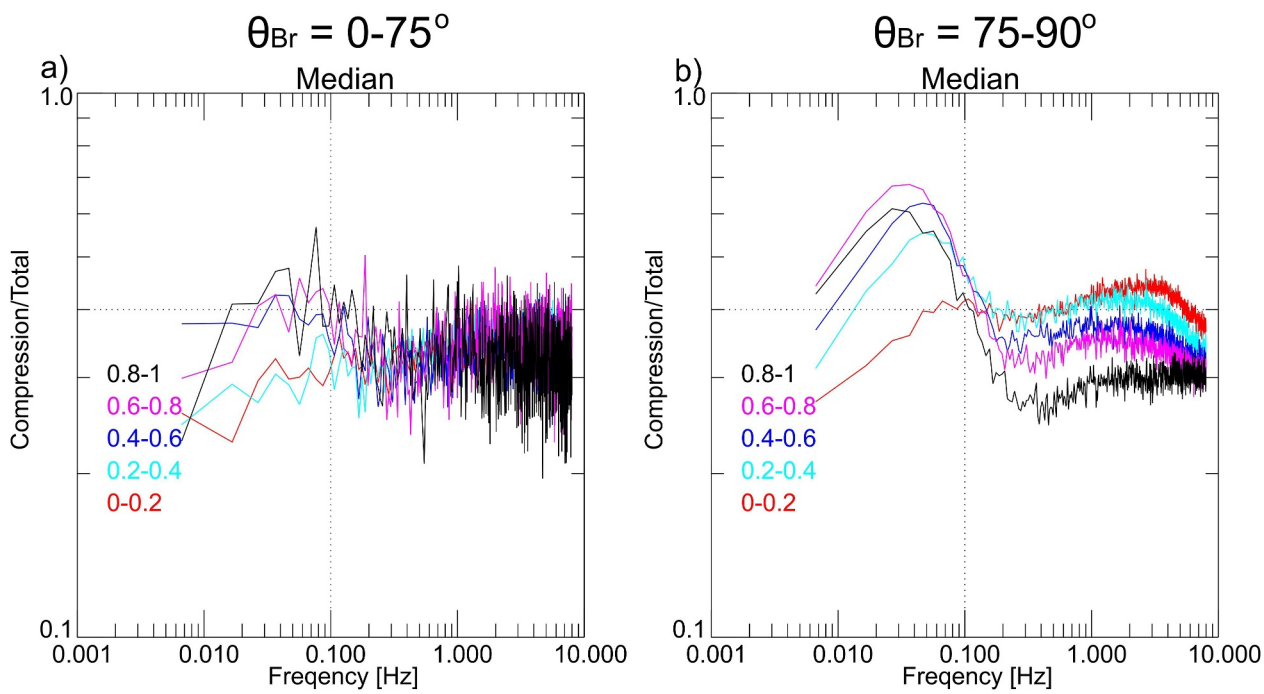

Figure 8. Superposed wave spectra in the same format as Figure 7 show the compressional component normalized by the total wave power.

In Figure 2, we use the total wave power from GMAG stations. Using only the north–south or east–west components slightly decreases the correlation in the $\theta_{Br} = 0$–$75°$ region slightly to 0.37 and 0.40, respectively. Using both the north–south and east–west components yields nearly the same correlation (0.41) as using all three components. Using only the vertical component reduces the correlation further to 0.30. These results resemble foreshock-to-ground relationships (Liu et al., 2025), suggesting that the ground responses are not purely poloidal or toroidal modes (e.g., Klimushkin et al., 2004).

Distinguishing between regions downstream of quasi-parallel and quasi-perpendicular bow shocks is important but challenging. Our study demonstrates that $\theta_{Br} = 75°$ is an effective criterion, likely because our events are not too far from the subsolar point (Figure 1f; otherwise, TH-A can hardly cross the entire magnetosheath due to limited apogee). This criterion is less reliable at the flanks, where field line draping and deviations of bow shock and magnetopause normals from the radial direction become more significant. Due to field line draping, this criterion also depends on the radial distance in the magnetosheath (e.g., Figure 2e). Therefore, a more comprehensive classification method may yield improved results.

In this study, spacecraft crossings were used to determine bow shock and magnetopause locations, providing more accurate estimates than empirical models, though still subject to uncertainties. For example, bow shock and magnetopause locations could change globally when TH-A traverses the magnetosheath due to solar wind variations. The bow shock and magnetopause thickness can also cause uncertainties. However, given our bin sizes (1/2–1/5 of the magnetosheath thickness), only extreme events, which are rare, could significantly affect the results.

Finally, ionospheric, atmospheric, and ground properties may also modulate magnetosheath-to-ground relationships (e.g., review by Southwood and Hughes (1983); Archer et al. (2023)). To test the potential role of ionospheric properties in wave transmission (e.g., Engebretson et al., 1991), Figure S7 in Supporting Information S1 examines seasonal dependence. Using the same data set as Figure 2, for $\theta_{Br} = 0$–$75°$, the correlation increases to 0.62 in June–July and decreases to 0.32 in August–December (with most events occurring between June and December due to THEMIS orbit configurations). Because the average spacecraft MLT is nearly the same (∼11 hr) during the two intervals, this correlation difference could be caused by seasonal variations in ionospheric properties. Further examinations will be essential for advancing our understanding of wave transmission to the ground.

5. Conclusions

Using $\theta_{Br} = 75°$ as a boundary within the magnetosheath, we identified two wave populations with distinct ground responses and wave characteristics. In the $\theta_{Br} = 0$–$75°$ region, approximately downstream of the quasi-parallel bow shock, magnetosheath magnetic wave power correlates with ground-based magnetic wave power at periods of ∼30s, with correlation coefficients reaching up to ∼0.7. The correlation is strongest when the spacecraft is close to the magnetopause and on the dawnside while GMAG stations are on the duskside (MLAT 50–60°) or on both sides (MLAT 40–50°). Radial dynamic pressure wave power also correlates well with ground-based magnetic wave power, with coefficients reaching up to ∼0.7.

In contrast, in the $\theta_{Br} = 75$–$90°$ region, approximately downstream of the quasi-perpendicular bow shock, magnetic field and radial dynamic pressure wave power show no or weak correlation with ground-based magnetic wave power. The correlation coefficients increase with decreasing frequency, reaching ∼0.3 at 6.67 mHz, and show no clear dependence on radial distance in the magnetosheath (except at 0.06 Hz). However, the joint dependence of the spacecraft and GMAG stations on the MLT exhibits some similarities to that in the $\theta_{Br} = 0$–$75°$ region, potentially suggesting general wave propagation patterns.

We also examine differences in wave properties between the two regions. (a) In the $\theta_{Br} = 0$–$75°$ region, magnetic wave power correlates with plasma wave power, with coefficients above 0.5, while in the $\theta_{Br} = 75$–$90°$ region, there is no or weak correlation (0–0.4). (b) In the $\theta_{Br} = 0$–$75°$ region, wave power below 0.1 Hz shows little radial evolution, whereas in the $\theta_{Br} = 75$–$90°$ region, wave power increases from the bow shock to the magnetopause and is weaker than that in the $\theta_{Br} = 0$–$75°$ region. (c) Waves in the $\theta_{Br} = 0$–$75°$ region are less compressive than those in the $\theta_{Br} = 75$–$90°$ region, and in both regions, compressibility generally increases deeper into the magnetosheath below 0.1 Hz. These results suggest that foreshock-induced waves likely dominate in the $\theta_{Br} = 0$–$75°$ region, in contrast to the $\theta_{Br} = 75$–$90°$ region.

Our results suggest that in the magnetosheath regions downstream of quasi-parallel bow shocks, foreshock-originated waves can effectively drive magnetospheric ULF waves at periods of ∼30s, through both magnetic field and dynamic pressure oscillations. These waves are transmitted preferentially from the dawnside magnetosheath toward both the duskside and dawnside of the magnetosphere. In contrast, downstream of quasi-perpendicular bow shocks, magnetosheath-generated waves and solar wind-originated waves show minimal contribution to magnetospheric Pc3–4 waves, which may require further separation of these wave populations.

Conflict of Interest

The authors declare no conflicts of interest relevant to this study.

Data Availability Statement

The THEMIS and GMAG data sets are available at NASA's Coordinated Data Analysis Web (CDAWeb, https://cdaweb.gsfc.nasa.gov/ and then select THEMIS). The SPEDAS software (see Angelopoulos et al., 2019) is available at https://themis.ssl.berkeley.edu/software.shtml. Our GMAG station list can also be found from the SPEDAS routine, thm_gmag_stations.pro.

Acknowledgments

T.Z.L. is partially supported by NSF award AGS-2247760 and NASA Grants 80NSSC23K0086, 80NSSC23K0903, and 80NSSC25K7684. S.D. is supported by NASA Grant 80NSSC20K0801. M.D.H is supported by NASA Grants 80NSSC23K0903 and 80NSSC24K1026 and NSF Grant AGS-2027210. S.R. acknowledges funding from the Johns Hopkins University Applied Physics Laboratory Independent R&D fund and from NASA DRIVE Science Center for Geospace Storms (CGS) under award 80NSSC22M0163. K.Z. is supported by NASA Grants 80NSSC24K0677 and 80NSSC25K7684 and NSF Grant AGS-2420710. We acknowledge the NASA THEMIS contract NAS5-02099, the SPEDAS team and NASA's Coordinated Data Analysis Web. We thank K. H. Glassmeier, U. Auster, and W. Baumjohann for the use of the THEMIS/FGM data provided under the lead of the Technical University of Braunschweig and with financial support through the German Ministry for Economy and Technology and the German Center for Aviation and Space (DLR) under contract 50 OC 0302. We also thank the late C. W. Carlson and J. P. McFadden for the use of THEMIS/ESA data.

References

Angelopoulos, V. (2008). The THEMIS mission. *Space Science Reviews*, *141*(1–4), 5–34. https://doi.org/10.1007/s11214-008-9336-1

Angelopoulos, V., Cruce, P., Drozdov, A., Grimes, E. W., Hatzigeorgiu, N., King, D. A., et al. (2019). The space physics environment data analysis system (SPEDAS) [Software]. *Space Science Reviews*, *215*(1), 9. https://doi.org/10.1007/s11214-018-0576-4

Archer, M. O., Hartinger, M. D., Rastätter, L., Southwood, D. J., Heyns, M., Eggington, J. W. B., et al. (2023). Auroral, ionospheric and ground magnetic signatures of magnetopause surface modes. *Journal of Geophysical Research: Space Physics*, *128*(3), e2022JA031081. https://doi.org/10.1029/2022JA031081

Auster, H. U., Glassmeier, K. H., Magnes, W., Aydogar, O., Baumjohann, W., Constantinescu, D., et al. (2008). The THEMIS fluxgate magnetometer. *Space Science Reviews*, *141*(1–4), 235–264. https://doi.org/10.1007/s11214-008-9365-9

Bloom, R. M., & Singer, H. J. (1995). Diurnal trends in geomagnetic noise power in the Pc 2 through Pc 5 bands at low geomagnetic latitudes. *Journal of Geophysical Research*, *100*(A8), 14943–14953. https://doi.org/10.1029/95JA01332

Burgess, D., Möbius, E., & Scholer, M. (2012). Ion acceleration at the Earth's bow shock. *Space Science Reviews*, *173*(1–4), 5–47. https://doi.org/10.1007/s11214-012-9901-5

Clausen, L. B. N., Yeoman, T. K., Fear, R. C., Behlke, R., Lucek, E. A., & Engebretson, M. J. (2009). First simultaneous measurements of waves generated at the bow shock in the solar wind, the magnetosphere and on the ground. In *Annales geophysicae*. Copernicus GmbH. https://doi.org/10.5194/angeo-27-357-2009

Eastwood, J. P., Lucek, E. A., Mazelle, C., Meziane, K., Narita, Y., Pickett, J., & Treumann, R. A. (2005). *The foreshock. Space science reviews*. Springer Science and Business Media LLC. https://doi.org/10.1007/s11214-005-3824-3

Edmiston, J. P., Kennel, C. F., & Eichler, D. (1982). Escape of heated ions upstream of quasi-parallel shocks. *Geophysical Research Letters*, *9*(5), 531–534. https://doi.org/10.1029/GL009i005p00531

Engebretson, M. J., Cahill, L. J., Jr., Arnoldy, R. L., Anderson, B. J., Rosenberg, T. J., Carpenter, D. L., et al. (1991). The role of the ionosphere in coupling upstream ULF wave power into the dayside magnetosphere. *Journal of Geophysical Research*, *96*(A2), 1527–1542. https://doi.org/10.1029/90JA01767

Engebretson, M. J., Zanetti, L. J., Potemra, T. A., Baumjohann, W., Lühr, H., & Acuna, M. H. (1987). Simultaneous observation of Pc 3–4 pulsations in the solar wind and in the Earth's magnetosphere. *Journal of Geophysical Research*, *92*(A9), 10053–10062. https://doi.org/10.1029/JA092iA09p10053

Eriksson, P. T. I., Walker, A. D. M., & Stephenson, J. A. E. (2006). A statistical correlation of Pc5 pulsations and solar wind pressure oscillations. *Advances in Space Research*, *38*(8), 1763–1771. https://doi.org/10.1016/j.asr.2005.08.023

Greenstadt, E. W., & Olson, J. V. (1976). Pc 3, 4 activity and interplanetary field orientation. *Journal of Geophysical Research*, *81*(34), 5911–5920. https://doi.org/10.1029/JA081i034p05911

Karlsson, T., Raptis, S., Trollvik, H., & Nilsson, H. (2021). Classifying the magnetosheath behind the quasi-parallel and quasi-perpendicular bow shock by local measurements. *Journal of Geophysical Research: Space Physics*, *126*(9), e2021JA029269. https://doi.org/10.1029/2021JA029269

Klimushkin, D. Y., Mager, P. N., & Glassmeier, K.-H. (2004). Toroidal and poloidal Alfvén waves with arbitrary azimuthal wavenumbers in a finite pressure plasma in the Earth's magnetosphere. *Annals of Geophysics*, *22*(1), 267–287. https://doi.org/10.5194/angeo-22-267-2004

Koller, F., Wedlund, C. S., Temmer, M., Svenningsson, I., Preisser, L., Pöppelwerth, A., et al. (2025). Stability of the Earth's dayside magnetosheath: Effects of upstream solar wind structures and downstream jets. *Journal of Geophysical Research: Space Physics*, *130*(9), e2025JA034098. https://doi.org/10.1029/2025JA034098

Krauss-Varban, D. (1995). Waves associated with quasi-parallel shocks: Generation, mode conversion and implications. *Advances in Space Research*, *15*(8–9), 271–284. https://doi.org/10.1016/0273-1177(94)00107-c

Lacombe, C., & Belmont, G. (1995). Waves in the Earth's magnetosheath: Observations and interpretations. *Advances in Space Research. Elsevier BV*, *15*(8–9), 329–340. https://doi.org/10.1016/0273-1177(94)00113-f

Liu, T. Z., Angelopoulos, V., Dorfman, S., Hartinger, M. D., Zhang, K., Raptis, S., & Ma, D. (2025). Statistical relationship between foreshock ULF wave power and ground-based Pc3-4 wave power. *Journal of Geophysical Research: Space Physics*, *130*(9), e2025JA033760. https://doi.org/10.1029/2025JA033760

Liu, T. Z., Angelopoulos, V., Vu, A., Zhang, H., Otto, A., & Zhang, K. (2024). THEMIS observations of magnetosheath-origin foreshock ions. *Journal of Geophysical Research: Space Physics*, *129*(2), e2023JA031969. https://doi.org/10.1029/2023JA031969

Liu, T. Z., Hao, Y., Wilson, L. B., III., Turner, D. L., & Zhang, H. (2021). Magnetospheric multiscale observations of Earth's oblique bow shock reformation by foreshock ultralow-frequency waves. *Geophysical Research Letters*, *47*(2), e2020GL091184. https://doi.org/10.1029/2020GL091184

McFadden, J. P., Carlson, C. W., Larson, D., Angelopoulos, V., Ludlam, M., Abiad, R., et al. (2008). The THEMIS ESA plasma instrument and in-flight calibration. *Space Science Reviews*, *141*(1–4), 277–302. https://doi.org/10.1007/s11214-008-9440-2

Merka, J., Szabo, A., Slavin, J. A., & Peredo, M. (2005). Three-dimensional position and shape of the bow shock and their variation with upstream Mach numbers and interplanetary magnetic field orientation. *Journal of Geophysical Research*, *110*(A4), A04202. https://doi.org/10.1029/2004JA010944

Omidi, N., O'Farrell, A., & Krauss-Varban, D. (1994). Sources of magnetosheath waves and turbulence. *Advances in Space Research. Elsevier BV*, *14*(7), 45–54. https://doi.org/10.1016/0273-1177(94)90047-7

Raptis, S., Karlsson, T., Plaschke, F., Kullen, A., & Lindqvist, P.-A. (2020). Classifying magnetosheath jets using MMS: Statistical properties. *Journal of Geophysical Research: Space Physics*, *125*(11), e2019JA027754. https://doi.org/10.1029/2019JA027754

Russell, C. T., Chi, P. J., Dearborn, D. J., Ge, Y. S., Kuo-Tiong, B., Means, J. D., et al. (2009). THEMIS ground-based magnetometers. In J. L. Burch & V. Angelopoulos (Eds.), *The THEMIS mission*. Springer. https://doi.org/10.1007/978-0-387-89820-9_17

Russell, C. T., Luhmann, J. G., Odera, T. J., & Stuart, W. F. (1983). The rate of occurrence of dayside Pc 3,4 pulsations: The L-value dependence of the IMF cone angle effect. *Geophysical Research Letters*, *10*(8), 663–666. https://doi.org/10.1029/GL010i008p00663

Shue, J.-H., Song, P., Russell, C. T., Steinberg, J. T., Chao, J. K., Zastenker, G., et al. (1998). Magnetopause location under extreme solar wind conditions. *Journal of Geophysical Research*, *103*(A8), 17691–17700. https://doi.org/10.1029/98JA01103

Sibeck, D. G., Baumjohann, W., Elphic, R. C., Fairfield, D. H., Fennell, J. F., Gail, W. B., et al. (1989). The magnetospheric response to 8-minute period strong-amplitude upstream pressure variations. *Journal of Geophysical Research*, *94*(A3), 2505–2519. https://doi.org/10.1029/JA094iA03p02505

Singer, H. J., Southwood, D. J., Walker, R. J., & Kivelson, M. G. (1981). Alfven wave resonances in a realistic magnetospheric magnetic field geometry. *Journal of Geophysical Research*, *86*(A6), 4589–4596. https://doi.org/10.1029/JA086iA06p04589

Sonnerup, B. U. Ö. (1969). Acceleration of particles reflected at a shock front. *Journal of Geophysical Research*, *74*(5), 1301–1304. https://doi.org/10.1029/JA074i005p01301

Soucek, J., Escoubet, C. P., & Grison, B. (2015). Magnetosheath plasma stability and ULF wave occurrence as a function of location in the magnetosheath and upstream bow shock parameters. *Journal of Geophysical Research: Space Physics*, *120*(4), 2838–2850. https://doi.org/10.1002/2015JA021087

Soucek, J., Lucek, E., & Dandouras, I. (2008). Properties of magnetosheath mirror modes observed by Cluster and their response to changes in plasma parameters. *Journal of Geophysical Research*, *113*(A4), A04203. https://doi.org/10.1029/2007JA012649

Southwood, D. J., & Hughes, W. J. (1983). Theory of hydromagnetic waves in the magnetosphere. *Space Science Reviews*, *35*(4), 301–366. https://doi.org/10.1007/BF00169231

Stephenson, J. A. E., & Walker, A. D. M. (2002). HF radar observations of Pc5 ULF pulsations driven by the solar wind. *Geophysical Research Letters*, *29*(9). https://doi.org/10.1029/2001gl014291

Svenningsson, I., Yordanova, E., Khotyaintsev, Y. V., André, M., & Cozzani, G. (2025). Classifying the magnetosheath using local measurements from MMS. *Journal of Geophysical Research: Space Physics*, *130*(1), e2024JA033272. https://doi.org/10.1029/2024JA033272

Takahashi, K., Chi, P. J., Denton, R. E., & Lysak, R. L. (Eds.) (2006). Magnetospheric ULF waves: Synthesis and new directions, *Geophysical monograph series*. American Geophysical Union. https://doi.org/10.1029/gm169

Takahashi, K., McPherron, R. L., & Terasawa, T. (1984). Dependence of the spectrum of Pc 3–4 pulsations on the interplanetary magnetic field. *Journal of Geophysical Research*, *89*(A5), 2770–2780. https://doi.org/10.1029/JA089iA05p02770

Takahashi, K., Turc, L., Kilpua, E., Takahashi, N., Dimmock, A., Kajdic, P., et al. (2021). Propagation of ultralow-frequency waves from the ion foreshock into the magnetosphere during the passage of a magnetic cloud. *Journal of Geophysical Research: Space Physics*, *126*(2), e2020JA028474. https://doi.org/10.1029/2020JA028474

Turc, L., Roberts, O. W., Verscharen, D., Dimmock, A. P., Kajdič, P., Palmroth, M., et al. (2023). Transmission of foreshock waves through Earth's bow shock. *Nature Physics*, *19*(1), 78–86. https://doi.org/10.1038/s41567-022-01837-z

Wilson, L. B., III. (2016). Low frequency waves at and upstream of collisionless shocks. In A. Keiling, D.-H. Lee, & V. Nakariakov (Eds.), *Low-frequency waves in space plasmas*. https://doi.org/10.1002/9781119055006.ch16

Zou, Y., Walsh, B. M., Chen, Y., Zhou, H., & Raptis, S. (2025). Control of solar wind on magnetic field fluctuations in the subsolar magnetosheath. *Journal of Geophysical Research: Space Physics*, *130*(6), e2025JA033856. https://doi.org/10.1029/2025JA033856